

# Laser-induced nonsequential double ionization in diatomic molecules: one and two-center rescattering scenarios

C. Figueira de Morisson Faria

**Abstract.** We investigate laser-induced nonsequential double ionization from aligned diatomic molecules, using the strong-field approximation in its length and velocity gauge formulations. Throughout, we consider that the first electron dislodges the second by electron-impact ionization. Employing modified saddle-point equations, we single out the contributions of different scattering scenarios to the maxima and minima observed in the differential electron momentum distributions. We show that the quantum interference between the electron orbits starting and ending at a specific center  $C_j$ , and those starting at  $C_j$  and ending at a different center  $C_\nu$ , leads to the same maxima as minima as if all possible scenarios are taken. There exist, however, quantitative differences as far as the gauge choice is concerned. Indeed, while the velocity-gauge distributions obtained employing only the above-mentioned processes are practically identical to the overall distributions, their length-gauge counterparts exhibit an asymmetry in the positive and negative momentum regions. This asymmetry is due to additional potential-energy shifts which are only present in the length-gauge formulation, and which, depending on the center, sink or increase the potential barrier through which the first electron tunnels. In contrast, the interference between topologically similar scenarios leads at most to patterns whose positions, in momentum space, do not agree with the overall interference condition, neither in the length nor in the velocity gauge.

PACS numbers: 32.80.Rm, 33.80.Rv  
Department of Physics and Astronomy, University College London,  
Gower Street, London WC1E 6BT, United Kingdom  
E-mail: c.faria@ucl.ac.uk

## 1. Introduction

Molecules in strong laser fields ( $I \sim 10^{14} - 10^{15} \text{W/cm}^2$ ) have been the object of intensive scrutiny in the past few years. In particular, high-order harmonic generation (HHG) and above-threshold ionization (ATI) have been employed to extract information about the structure of such systems with subfemtosecond precision [1]. This is made possible by the physical mechanisms behind such phenomena, namely the rescattering or recombination of the active electron with its parent molecule [2]. These processes take place within a fraction of a laser cycle. For a typical Titanium-Sapphire laser field, whose cycle is roughly  $T \sim 2.7 \text{fs}$ , this corresponds to hundreds of attoseconds [3]. In particular, the configuration of atoms with which the electron rescatters or recombines leads to patterns which are characteristic of the molecule. These patterns may be either due to the quantum interference of photoelectron

or harmonic emission in spatially separated centers [4], or of the rescattering or recombination scenarios involving more than one center [5, 6, 7, 8, 9, 10, 11].

Specifically for ATI and HHG in diatomic molecules, there exist analytic expressions which give the approximate energy positions of the interference minima and maxima due to the above-mentioned spatial separation [4]. This allows a physical interpretation in terms of a microscopic double-slit experiment. In particular in the framework of semi-analytic, S-Matrix approaches, such as the strong-field approximation (SFA), the HHG or ATI transition amplitudes are written as multiple integrals, with slowly-varying prefactors and a semiclassical action [12]. In this case, the double-slit interference appears as a prefactor, which depends on the symmetry of the highest occupied molecular orbital and on the internuclear distance [5, 6, 7, 8, 9, 11, 13, 14, 15, 16, 18, 17].

There are, however, comparatively fewer studies of the influence of two-center scenarios, in which an electron is released in a center  $C_j$  in the molecule and rescatters or recombines with a different center  $C_\nu$ ,  $j \neq \nu$  [5, 6, 7, 8, 9, 10]. In these references, the two-center processes have also been treated and discussed in quite different ways. For instance, in [7, 9, 10], the high-order harmonic double-slit prefactor has been exponentialized and incorporated in the action, while in high-order ATI the two-center processes led to transition amplitudes, which could not be grouped as to provide a common prefactor [8].

In previous work, we have shown that well-defined interference fringes may be also present in laser-induced nonsequential double ionization (NSDI) of diatomic molecules [19], for a small range of alignment angles. This is a consequence of the fact that NSDI is also described as a laser-induced rescattering process. More specifically, the first electron, freed at a time  $t'$ , is accelerated by the external laser field and, at a subsequent time  $t$ , collides inelastically with its parent molecule. In this collision, it gives part of the kinetic energy it acquired from the field to a second electron, which is then released. Quantum mechanically, transition amplitudes corresponding to NSDI at different centers in the molecule are expected to interfere. Even though, up to the present date, there is no experimental evidence of such fringes, recently, it has been observed that the shapes and the peaks of the NSDI differential electron momentum distributions in molecules depend on the symmetry of the highest occupied molecular orbital [20], and on the molecular alignment angle with respect to the laser-field polarization [21].

In [19], we worked mainly within the SFA, and assumed that the second electron was dislodged by the simplest possible physical mechanism: electron-impact ionization. We have shown that, in this case, the two-center interference leads to minima and maxima parallel to the anti-diagonal  $p_{(1)\parallel} + p_{(2)\parallel}$  in the plane of the momentum components  $(p_{(1)\parallel}, p_{(2)\parallel})$  parallel to the laser-field polarization. For parallel-aligned molecules, these fringes are sharpest. As the alignment angle increases, the contributions from the perpendicular momentum components start to blur these fringes, until, for perpendicular alignment, all structure is washed out. In such investigations, we incorporated the structure of the molecule in the prefactor, and kept the same action as in the single-atom case.

A legitimate question is, however, how the different rescattering scenarios, involving one or two centers, contribute to the above-mentioned patterns in NSDI. In the following, we will address this issue, incorporating the prefactors derived in [19] in the semiclassical action. A closely related procedure has been followed in [7, 9], for high-order harmonic generation. In order to facilitate this assessment and make

the two-center interference fringes as clear as possible, we strip the problem to its bare bones using a series of assumptions. Firstly, unless otherwise stated, we consider very simplified highest occupied molecular orbitals, for which analytic interference conditions have been derived [19]. Furthermore, we choose the interaction through which the second electron is dislodged as a contact-type interaction at the positions of the ions. As it will be discussed subsequently (c.f. Sec. 3), this type of interaction eliminates any bias in the electron momentum distributions, which may be detrimental for their interpretation<sup>‡</sup>. Finally, throughout, we will consider the condition for which the interference patterns are most pronounced, i.e., parallel alignment.

This paper is organized as follows. In Sec. 2, we give the expression for the transition amplitude related to the process in which the second electron is freed by electron-impact ionization, within the SFA. We also briefly recall the two-center prefactors employed in [19], and the expression derived in Ref. [19] for the two-center NSDI interference conditions (Sec. 2.2). Subsequently, in Sec. 2.3, we provide the expressions for the modified saddle-point equations, in which different scattering processes are taken into account. In Sec. 3, these equations are employed to compute differential momentum distributions, which are analyzed in detail. Finally, in Sec. 4, we summarize the paper and provide its main conclusions.

## 2. Transition amplitudes

### 2.1. General expressions

The simplest process responsible for laser-induced nonsequential double ionization is electron-impact ionization. Within the Strong-Field Approximation, the corresponding transition amplitude is given by

$$M(\mathbf{p}_{(1)}, \mathbf{p}_{(2)}) = \int_{-\infty}^{\infty} dt \int_{-\infty}^t dt' \int d^3k V_{\{\mathbf{p}_{(n)}\}k} V_{k0} \exp[iS(\{\mathbf{p}_{(n)}\}, \mathbf{k}, t, t')], \quad (1)$$

with

$$S(\{\mathbf{p}_{(n)}\}, \mathbf{k}, t, t') = - \sum_{n=1}^2 \int_t^{\infty} \frac{[\mathbf{p}_{(n)} + \mathbf{A}(\tau)]^2}{2} d\tau - \int_{t'}^t \frac{[\mathbf{k} + \mathbf{A}(\tau)]^2}{2} d\tau - E_{0(2)}t - E_{0(1)}t' \quad (2)$$

and the prefactors

$$V_{\mathbf{k}0} = \langle \tilde{\mathbf{k}}(t') | V | \phi_0^{(1)} \rangle \quad (3)$$

and

$$V_{\{\mathbf{p}_{(n)}\}\mathbf{k}} = \langle \tilde{\mathbf{p}}_{(1)}(t), \tilde{\mathbf{p}}_{(2)}(t) | V_{12} | \tilde{\mathbf{k}}(t), \phi_0^{(2)} \rangle, \quad (4)$$

where the indices in parentheses are related to each electron involved and the term  $\{\mathbf{p}_{(n)}\}$  in brackets is related to *both* electron momenta. Eq. (1) describes the process in which an electron, initially in a bound state  $|\phi_0^{(1)}\rangle$ , is freed by tunneling ionization at a time  $t'$  into a Volkov state  $|\tilde{\mathbf{k}}(t)\rangle$ . Subsequently, this electron propagates in the continuum from  $t'$  to a later time  $t$ . At this time, the electron collides inelastically with

<sup>‡</sup> Apart from that, in the single-atom case and within the SFA framework, this type of interaction led to a better agreement with the existing experiments than more realistic choices, such as a Coulomb-type interaction. For a detailed discussion, see Refs. [24, 25].

its parent molecule, and a second electron, which is bound in  $|\phi_0^{(2)}\rangle$ , is then released through the interaction  $V_{12}$ . Thereafter, both electrons are in Volkov states, and their final momenta are  $\mathbf{p}_{(n)}(n = 1, 2)$ . In the above-stated equations,  $E_{0(n)}(n = 1, 2)$  give the first and second ionization potentials, and  $V$  the atomic potential. The form factors (3) and (4) contain all the information about the atomic potential, and the interaction by which the second electron is dislodged (see [24] for details). One should note that the transition amplitude cannot be factorized into one-electron transition amplitudes. Physically, this implies a strongly correlated two-electron process.

Another noteworthy issue is that, within the SFA,  $V_{\mathbf{k}0}$  and  $V_{\{\mathbf{p}_{(n)}\}\mathbf{k}}$  are gauge dependent. In fact, in the length gauge  $\tilde{\mathbf{p}}_{(n)}(\tau) = \mathbf{p}_{(n)} + \mathbf{A}(\tau)$  and  $\tilde{\mathbf{k}}(\tau) = \mathbf{k} + \mathbf{A}(\tau)$  ( $\tau = t, t'$ ), while in the velocity gauge  $\tilde{\mathbf{p}}_{(n)}(\tau) = \mathbf{p}_{(n)}$  and  $\tilde{\mathbf{k}}(\tau) = \mathbf{k}$ . A similar gauge dependence has also been reported for high-order harmonic generation [7, 9] and above-threshold ionization [18, 11]. For a more general discussion see [22].

## 2.2. Two-center prefactors

In the specific case of diatomic molecules, we will consider the same simplified model as in [19], namely frozen nuclei, the linear combination of atomic orbitals (LCAO) approximation, and homonuclear molecules. Under these assumptions, the molecular bound-state wave function for each electron reads

$$\psi_0^{(n)}(\mathbf{r}_{(n)}) = C_\psi \left[ \phi_0^{(n)}(\mathbf{r}_{(n)} - \mathbf{R}/2) + \epsilon \phi_0^{(n)}(\mathbf{r}_{(n)} + \mathbf{R}/2) \right], \quad (5)$$

where  $n = 1, 2$ ,  $\epsilon = \pm 1$ , and  $C_\psi = 1/\sqrt{2(1 + \epsilon S(\mathbf{R}))}$ , with

$$S(\mathbf{R}) = \int \left[ \phi_0^{(n)}(\mathbf{r}_{(n)} - \mathbf{R}/2) \right]^* \phi_0^{(n)}(\mathbf{r}_{(n)} + \mathbf{R}/2) d^3 r. \quad (6)$$

The positive and negative signs for  $\epsilon$  correspond to bonding and antibonding orbitals, respectively.

The molecular binding potential, as seen by each electron, is written as

$$V(\mathbf{r}_{(n)}) = V_0(\mathbf{r}_{(n)} - \mathbf{R}/2) + V_0(\mathbf{r}_{(n)} + \mathbf{R}/2), \quad (7)$$

where  $V_0$  corresponds to the binding potential of each center in the molecule, which, at this stage, are kept general. The above-stated assumptions yield

$$V_{\mathbf{k}0}^{(b)} = -\frac{2C_\psi}{(2\pi)^{3/2}} \cos[\tilde{\mathbf{k}}(t') \cdot \mathbf{R}/2] \mathcal{I}(\tilde{\mathbf{k}}(t')) \quad (8)$$

or

$$V_{\mathbf{k}0}^{(a)} = -\frac{2iC_\psi}{(2\pi)^{3/2}} \sin[\tilde{\mathbf{k}}(t') \cdot \mathbf{R}/2] \mathcal{I}(\tilde{\mathbf{k}}(t')), \quad (9)$$

for the bonding and antibonding cases, respectively, with

$$\mathcal{I}(\tilde{\mathbf{k}}(t')) = \int d^3 r_{(1)} \exp[i\tilde{\mathbf{k}}(t') \cdot \mathbf{r}_{(1)}] V_0(\mathbf{r}_{(1)}) \phi_0^{(1)}(\mathbf{r}_{(1)}). \quad (10)$$

In the above-stated equations, we have neglected the integrals for which the binding potential and the bound-state wave function are localized at different centers in the molecule, due to the fact that they are very small for the parameter range of interest.

If the electron-electron interaction depends only on the distance between the two electrons, i.e.,  $V_{12} = V(\mathbf{r}_{(1)} - \mathbf{r}_{(2)})$ , the prefactor  $V_{\{\mathbf{p}_{(n)}\}\mathbf{k}}$  reads

$$V_{\{\mathbf{p}_{(n)}\}\mathbf{k}}^{(b)} = \frac{2C_\psi}{(2\pi)^{9/2}} V(\mathbf{p}_{(1)} - \mathbf{k}) \cos[\mathcal{P}(t) \cdot \mathbf{R}/2] \varphi_0^{(2)}(\mathcal{P}(t)) \quad (11)$$

or

$$V_{\{\mathbf{p}_{(n)}\}\mathbf{k}}^{(a)} = \frac{2iC_\psi}{(2\pi)^{9/2}} V(\mathbf{p}_{(1)} - \mathbf{k}) \sin[\mathcal{P}(t) \cdot \mathbf{R}/2] \varphi_0^{(2)}(\mathcal{P}(t)), \quad (12)$$

with  $\mathcal{P}(t) = \tilde{\mathbf{p}}_{(1)}(t) + \tilde{\mathbf{p}}_{(2)}(t) - \tilde{\mathbf{k}}(t)$ , for bonding and antibonding orbitals, respectively. Thereby,

$$\varphi_0^{(2)}(\mathcal{P}(t)) = \int d^3r_{(2)} \exp[i\mathcal{P}(t) \cdot \mathbf{r}_{(2)}] \phi_0^{(2)}(\mathbf{r}_{(2)}), \quad (13)$$

and

$$V(\mathbf{p}_{(1)} - \mathbf{k}) = \int d^3r V(\mathbf{r}) \exp[i(\mathbf{p}_{(1)} - \mathbf{k}) \cdot \mathbf{r}], \quad (14)$$

with  $\mathbf{r} = \mathbf{r}_{(1)} - \mathbf{r}_{(2)}$ . In the velocity and length gauges, the argument in Eqs. (11), (12) is given by  $\mathcal{P}(t) = \mathbf{p}_{(1)} + \mathbf{p}_{(2)} - \mathbf{k}$  and  $\mathcal{P}(t) = \mathbf{p}_{(1)} + \mathbf{p}_{(2)} - \mathbf{k} + \mathbf{A}(t)$ , respectively.

In terms of the momentum components  $p_{(n)\parallel}$ , or  $p_{(n)\perp}$  ( $n = 1, 2$ ), parallel and perpendicular to the laser-field polarization, condition (11) or (12) may be written as  $\cos[(\zeta_{\parallel} + \zeta_{\perp})R/2]$  or  $\sin[(\zeta_{\parallel} + \zeta_{\perp})R/2]$ , respectively, with

$$\zeta_{\parallel} = \left[ \sum_{i=1}^2 p_{(i)\parallel} - \kappa(t) \right] \cos \theta, \quad (15)$$

and

$$\zeta_{\perp} = p_{(1)\perp} \sin \theta \cos \varphi + p_{(2)\perp} \sin \theta \cos(\varphi + \alpha). \quad (16)$$

Thereby, the term  $\kappa(t)$  is equal to  $k - A(t)$  in the length gauge and to  $k$  in the velocity gauge. Eq. (15) provides well-defined interference fringes, as functions of the parallel momenta ( $p_{(1)\parallel}, p_{(2)\parallel}$ ). Eq. (16), on the other hand, has no obvious dependence on the alignment angle  $\theta$ . Indeed, because it depends on the angles  $\varphi$  and  $\alpha$ , in the momentum plane spanned by the perpendicular momentum components, when one integrates over such variables, its main effect is to blur the interference fringes. In this work, we will consider parallel-aligned molecules. This implies that Eq. (16) vanishes, and therefore that the interference patterns are sharpest. Explicitly, the interference conditions will be given by

$$p_{(1)\parallel} + p_{(2)\parallel} = \frac{N\pi}{R} + \kappa(t), \quad (17)$$

where  $N$  is an integer. For a symmetric combination of atomic orbitals, even or odd  $N$  gives the interference maxima and the minima, respectively, while in the antisymmetric case the situation is reversed.

### 2.3. Modified saddle-point equations

We will now incorporate the structure of the molecule, which is embedded in the prefactors (8)-(12), in the semiclassical action. Subsequently, the transition amplitudes obtained will be computed employing a uniform saddle-point approximation (c.f. [23] for details). For that purpose, we will exponentialize the prefactors  $V_{\mathbf{k}0}$  and  $V_{\{\mathbf{p}_{(n)}\}\mathbf{k}}$ . This procedure allows one to single out different rescattering scenarios, involving one or two centers.

This yields the sum

$$M = \sum_{j=1}^2 \sum_{\nu=1}^2 M_{j\nu} \quad (18)$$

of the transition amplitudes

$$M_{j\nu} = \int_{-\infty}^{\infty} dt \int_{-\infty}^t dt' \int d^3k \varphi_0^{(2)}(\mathcal{P}(t)) \mathcal{I}(\tilde{\mathbf{k}}(t')) \exp[iS_{j\nu}(\{\mathbf{p}_{(n)}\}, \mathbf{k}, t, t')], \quad (19)$$

with the modified action  $S_{j\nu}(\{\mathbf{p}_{(n)}\}, \mathbf{k}, t, t')$  defined as

$$S_{j\nu}(\{\mathbf{p}_{(n)}\}, \mathbf{k}, t, t') = S(\{\mathbf{p}_{(n)}\}, \mathbf{k}, t, t') + (-1)^\nu \left[ \mathcal{P}(t) + (-1)^{j+\nu} \tilde{\mathbf{k}}(t') \right] \cdot \frac{\mathbf{R}}{2}, \quad (20)$$

where the indices  $j, \nu$  relate to the centers in the molecule. In the above-stated equation, for processes involving a single center,  $j + \nu$  is even, while for scattering scenarios in which the first electron leaves at a center  $C_j$  and rescatters with a center  $C_\nu, \nu \neq j, j + \nu$  is odd. The saddle-point equations  $\partial_t S_{j\nu}(\{\mathbf{p}_{(n)}\}, \mathbf{k}, t, t') = \partial_{t'} S_{j\nu}(\{\mathbf{p}_{(n)}\}, \mathbf{k}, t, t') = 0$  and  $\partial_{\mathbf{k}} S_{j\nu}(\{\mathbf{p}_{(n)}\}, \mathbf{k}, t, t') = \mathbf{0}$  are explicitly given by

$$\frac{[\mathbf{k} + \mathbf{A}(t')]^2}{2} = -E_{0(1)} + (-1)^{2\nu+j+1} \partial_{t'} \tilde{\mathbf{k}}(t') \cdot \mathbf{R}/2, \quad (21)$$

$$\int_{t'}^t d\tau [\mathbf{k} + \mathbf{A}(\tau)] + (-1)^\nu \partial_{\mathbf{k}} \left\{ \left[ (-1)^{j+\nu} \tilde{\mathbf{k}}(t') - \tilde{\mathbf{k}}(t) \right] \cdot \mathbf{R}/2 \right\} = 0, \quad (22)$$

and

$$\sum_{n=1}^2 \frac{[\mathbf{p}_{(n)} + \mathbf{A}(t)]^2}{2} = \frac{[\mathbf{k} + \mathbf{A}(t)]^2}{2} - E_{0(2)} + (-1)^{\nu+1} \partial_t \mathcal{P}(t) \cdot \mathbf{R}/2. \quad (23)$$

Eq. (21) expresses the conservation of energy at  $t'$ , with tunneling ionization of the first electron. Eq. (22) provides the condition for the first electron to return, either to the site of its release or to the other ion. Finally, Eq. (23) yields the conservation of energy at the instant of rescattering.

One should note that the saddle-point equations (21) and (23) are gauge dependent. Specifically, in the length gauge, the tunneling and rescattering conditions are given by

$$\frac{[\mathbf{k} + \mathbf{A}(t')]^2}{2} = -E_{0(1)} + (-1)^{2\nu+j} \mathbf{E}(t') \cdot \mathbf{R}/2 \quad (24)$$

and

$$\sum_{n=1}^2 \frac{[\mathbf{p}_{(n)} + \mathbf{A}(t)]^2}{2} = \frac{[\mathbf{k} + \mathbf{A}(t)]^2}{2} - E_{0(2)} + (-1)^\nu \mathbf{E}(t) \cdot \mathbf{R}/2 \quad (25)$$

respectively. Physically, the additional terms in Eqs. (24) and (25) may be interpreted as potential-energy shifts, which sink or increase the ionization potentials. For instance, for single-center processes ( $j = \nu$ ), such shifts are symmetric, whereas for two-center scattering scenarios ( $j \neq \nu$ ) they possess the same sign. In the velocity gauge, the corresponding equations read

$$[\mathbf{k} + \mathbf{A}(t')]^2 = -2E_{0(1)}, \quad (26)$$

and

$$\sum_{n=1}^2 \frac{[\mathbf{p}_{(n)} + \mathbf{A}(t)]^2}{2} = \frac{[\mathbf{k} + \mathbf{A}(t)]^2}{2} - E_{0(2)}, \quad (27)$$

respectively. Eq. (26) and (29) are identical to the NSDI saddle-point equations for a single atom expressing tunneling ionization at  $t'$  and conservation of energy at  $t$ . Furthermore, in the limit  $E_{0(1)} \rightarrow 0$ , Eq. (26) may be interpreted as the initial kinetic energy of a classical particle, which starts its motion with vanishing drift momentum.

If written in terms of the electron momentum components parallel and perpendicular to the laser-field polarization, the rescattering conditions (25) and (27) read

$$\sum_{n=1}^2 \frac{[p_{(n)\parallel} + A(t)]^2}{2} + \frac{\mathbf{p}_{(n)\perp}^2}{2} = \frac{[\mathbf{k} + \mathbf{A}(t)]^2}{2} - \tilde{E}_{0(2)}. \quad (28)$$

In the length and velocity gauges,  $\tilde{E}_{0(2)} = E_{0(2)} + (-1)^\nu \mathbf{E}(t) \cdot \mathbf{R}/2$  and  $\tilde{E}_{0(2)} = E_{0(2)}$ , respectively. In the former case,  $\tilde{E}_{0(2)}$  can be viewed as an effective second ionization potential. The above-stated expression gives the equation of a six-dimensional hypersphere in momentum space, whose radius corresponds to the momentum region for which electron-impact ionization has a classical counterpart. If the kinetic energy of the first electron, upon return, is smaller than  $\tilde{E}_{0(2)}$ , then the second electron cannot be released and this process is classically forbidden. In this case, the corresponding transition probability is vanishingly small.

The return condition, and how it is related to such indices, can be clearly seen in Eq. (22). In fact, if  $j = \nu$ , the additional terms vanish, and the condition

$$\int_{t'}^t d\tau [\mathbf{k} + \mathbf{A}(\tau)] = 0, \quad (29)$$

is obtained. Eq. (29) constrains the value of the intermediate momentum  $\mathbf{k}$  so that the electron is leaving and returning to the same center in the molecule. On the other hand, if  $j \neq \nu$ , Eq. (22) reads

$$\int_{t'}^t d\tau [\mathbf{k} + \mathbf{A}(\tau)] + (-1)^{\nu+1} \mathbf{R} = 0. \quad (30)$$

The negative and the positive sign corresponds to the situation in which the electron starts from the center  $C_1$  and rescatters with  $C_2$ , or starts from  $C_2$  and rescatters with  $C_1$ , respectively. Both Eq. (29) and Eq. (22) are identical to the return conditions obtained from the classical equations of motion of an electron starting its orbit with vanishing drift momentum, and propagating under the influence of solely the laser field.

One should note that, within the context of high-order harmonic generation and above-threshold ionization, the additional potential-energy shifts present in the length-gauge SFA have raised a great deal of controversy. Indeed, there has been considerable debate whether such shifts are not an artifact of the strong-field approximation. Their existence is mainly related to the fact that the ions in the molecule are at a distance  $\pm \mathbf{R}/2$  from the origin of the coordinate system, which is located at the geometric center of the molecule [26, 28]. Furthermore, their presence does not allow an immediate connection with the classical equations of motion of an electron in an external laser field, as in the velocity-gauge formulation. For the above-stated reasons, it was suggested that these additional phase shifts should be removed by dressing the electronic bound states [28].

In recent HHG computations, however, it has been found that, if the additional potential-energy shifts are removed by employing field-dressed states, the two-center interference patterns break down [9, 27]. A direct comparison with the numerical

solution of the time-dependent Schrödinger equation has shown that this should only occur for very large internuclear distances, for which the atoms constituting the molecule practically behave as isolated entities [29]. Unfortunately, for NSDI, there are neither realistic computations by other means nor enough experiments to settle the issue. Therefore, in the following, we will compute electron momentum distributions in both length and velocity gauges without favoring any of them.

### 3. Electron momentum distributions

We will approximate the external laser field by a monochromatic wave  $\mathbf{E}(t) = \varepsilon_0 \sin \omega t \mathbf{e}_x$ . In this case, the electron momentum distributions, as functions of the momentum components  $(p_{(1)\parallel}, p_{(2)\parallel})$  parallel to the laser-field polarization, read

$$F(p_{(1)\parallel}, p_{(2)\parallel}) = \iint d^2 p_{(1)\perp} d^2 p_{(2)\perp} |M_R(\mathbf{p}_{(1)}, \mathbf{p}_{(2)}) + M_L(\mathbf{p}_{(1)}, \mathbf{p}_{(2)})|^2, \quad (31)$$

where the indices  $R$  and  $L$  denote the right and left peaks, respectively. The amplitude  $M_R$  is given by Eq. (1), and  $M_L(\mathbf{p}_{(1)}, \mathbf{p}_{(2)}) = M_R(-\mathbf{p}_{(1)}, -\mathbf{p}_{(2)})$ . In  $M_L(\mathbf{p}_{(1)}, \mathbf{p}_{(2)})$ , the action, the field and prefactors are displaced by half a cycle with respect to  $M_R$ , i.e., we used the symmetry  $\mathbf{A}(t) = \pm \mathbf{A}(t \pm T/2)$ .

The above-mentioned symmetry will guarantee that the overall electron momentum distributions, obtained either using the prefactor (8)-(12) or all four different transition amplitudes, will be symmetric with regard to the simultaneous inversion  $(p_{(1)\parallel}, p_{(2)\parallel}) \rightarrow (-p_{(1)\parallel}, -p_{(2)\parallel})$  of the parallel momentum components. Specifically for the transition amplitudes  $M_{j\nu}$ , we observe that  $M_{j\nu}(\mathbf{p}_{(1)}, \mathbf{p}_{(2)}) = M_{\nu j}(-\mathbf{p}_{(1)}, -\mathbf{p}_{(2)})$ . If both start and rescattering times  $t, t'$  were real, this would lead to symmetric distributions upon  $(p_{(1)\parallel}, p_{(2)\parallel}) \rightarrow (-p_{(1)\parallel}, -p_{(2)\parallel})$ . Furthermore, this would also guarantee that  $|M_{11} + M_{12}|^2 = |M_{22} + M_{21}|^2$  and  $|M_{12} + M_{22}|^2 = |M_{11} + M_{21}|^2$ . Since, however, the first electron is released through tunneling ionization,  $\text{Im}[t'] \neq 0$  and this is not necessarily so. This issue is particularly important in the length-gauge formulation of the SFA, and will be discussed subsequently.

In the form factor  $V_{\mathbf{k}0}$ , we considered Coulomb-type binding potentials  $V_0$  and a symmetric combination of  $1s$  orbitals. We assume that the second electron is dislodged by a contact-type interaction  $V_{12}$  placed at the position of the ions. Explicitly,

$$V_{12} = \delta(\mathbf{r}_{(1)} - \mathbf{r}_{(2)}) [\delta(\mathbf{r}_{(2)} - \mathbf{R}/2) + \delta(\mathbf{r}_{(2)} + \mathbf{R}/2)], \quad (32)$$

and can be viewed as an effective interaction, which in a rough way, accounts for the presence of the residual ions. This interaction has been employed in Ref. [19], within a two-center context, and has also been widely used in the single-atom case [24, 25]. In the specific context of this work, it has the advantage of eliminating any additional momentum dependence from  $\varphi_0^{(2)}(\mathcal{P}(t))$ , whose effect could be hard to disentangle from the two-center interference.

Throughout, we employ a higher driving-field intensity than those reported in typical NSDI experiments involving diatomic molecules [20, 21]. This has been done with the purpose of extending the region in momentum space for which electron-impact ionization exhibits a classical counterpart, i.e., the radius of the hypersphere (28). In previous work, we have shown that this was necessary in order to make a detailed assessment of quantum-interference effects in this context [19]. Furthermore, we restrict ourselves to the case of a symmetric combination of  $1s$  orbitals. This gives, for the specific interaction (32),

$$V_{\{\mathbf{p}_{(n)}\}\mathbf{k}} \sim \cos[\mathcal{P}(t) \cdot \mathbf{R}/2] \psi_{100}(0) \quad (33)$$



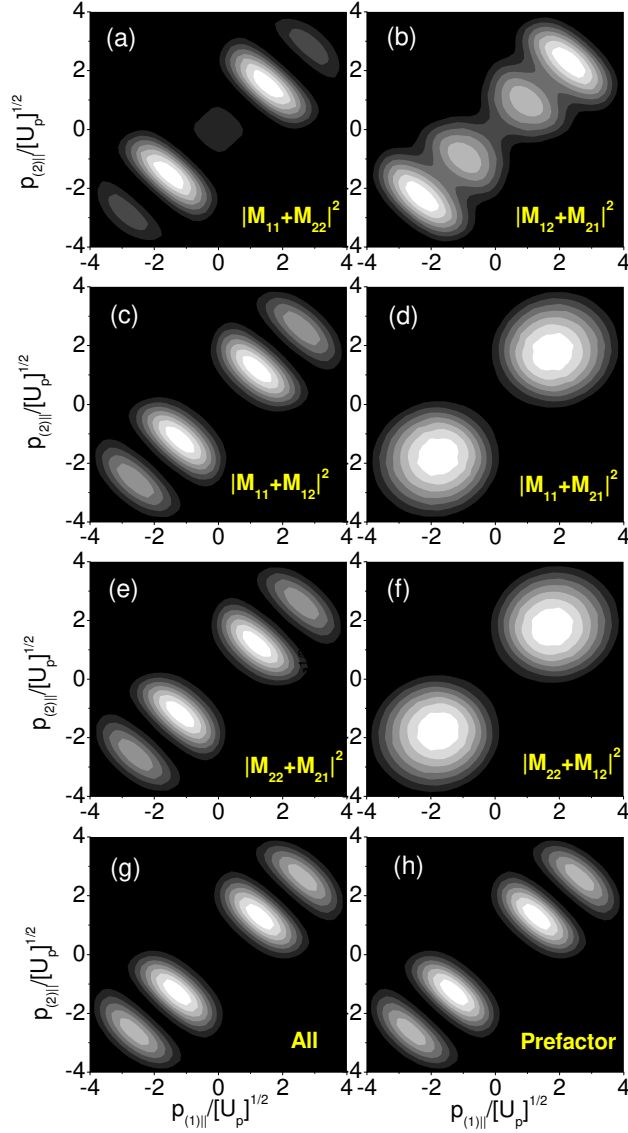


**Figure 1.** Contributions from different scattering scenarios to the electron momentum distributions as functions of the momentum components  $(p_{(1)||}, p_{(2)||})$  parallel to the laser-field polarization. The distributions have been computed in the velocity gauge and for a symmetric combination of 1s orbitals. The field intensity and frequency have been taken as  $I = 1.5 \times 10^{14} \text{ W/cm}^2$ , and  $\omega = 0.057$  a.u., respectively, and the ionization potentials  $E_{01} = 0.57$  a.u. and  $E_{02} = 0.98$  a.u. correspond to  $N_2$  at the equilibrium internuclear distance  $R = 2.068$  a.u. The upper panels display the contributions from topologically similar scattering scenarios, involving only one or two centers, i.e., the transition probabilities  $|M_{11} + M_{22}|^2$  and  $|M_{12} + M_{21}|^2$  [panels (a) and (b), respectively]. In panels (c) and (d), we display the contributions from the processes starting and ending at center  $C_1$ , respectively (transition probabilities  $|M_{11} + M_{12}|^2$  and  $|M_{11} + M_{21}|^2$ , respectively). Panels (e) and (f) depict the contributions  $|M_{21} + M_{22}|^2$  and  $|M_{12} + M_{22}|^2$  from those starting and ending at  $C_2$ , respectively. The sum  $|M_{11} + M_{12} + M_{21} + M_{22}|^2$  of all contributions are provided in panel (g). For comparison, panel (h) has been computed using the symmetric prefactors (8) and (11) and single-atom saddle-point equations.

Without loss of generality, however, our studies, as well as the conclusions of this work, may be extended to the antisymmetric case, or to more complex orbitals. In particular, if the interaction (32) is taken, only the contributions from s states would be non-vanishing in the form factor  $V_{\{\mathbf{p}_{(n)}\}\mathbf{k}}$ .

In Fig. 1, we display the electron momentum distributions in the velocity gauge and for symmetric orbitals, considering specific scattering processes. For comparison, in Fig. 1.(h), we are presenting the distributions obtained employing the prefactors (8) and (11) and solving single-atom saddle point equations. This approach has been considered in [19], and incorporates all the structure of the molecule in the prefactors. This distribution exhibits fringes in agreement with the interference condition (17).

In Fig. 1.(a), only the contributions from the processes in which the first electron leaves and returns to the same center have been taken into account. These processes are related to the transition amplitudes  $M_{jj}$  ( $j = 1, 2$ ). In this case, fringes parallel to the anti-diagonal  $p_{(1)||} = -p_{(2)||}$  are also present. Their position, however, disagrees with condition (17). A closer inspection, however, shows that the terms  $M_{11}$  and  $M_{22}$  can be grouped as  $\cos[(\mathbf{p}_{(1)} + \mathbf{p}_{(2)}) \cdot \mathbf{R}/2]$ . This gives another interference condition in terms of the parallel momentum components, namely  $p_{(1)||} + p_{(2)||} = N\pi/R$ . Maxima and minima are present for even and odd  $N$ , respectively. We have verified that all maxima and minima in the figure are approximately given by the above-stated expression, and correspond to the integers  $0 \leq N \leq 4$ .

If only the two-center processes are taken [Fig. 1.(b)], the transition amplitudes  $M_{21}$  and  $M_{12}$  can be grouped as  $\cos[(\mathbf{p}_{(1)} + \mathbf{p}_{(2)} - 2\mathbf{k}) \cdot \mathbf{R}/2]$ . This gives fringes following  $p_{(1)||} + p_{(2)||} - 2k = N\pi/R$ , which, once more, differ from the global interference condition (17). A rough analytic estimate of the position of the fringes can be made, by considering that the first electron leaves at peak field and returns at a field crossing. In this estimate, instead of using the modified return conditions (30), we considered the saddle-point equation (29), which states that the electron returns to the site of its release. In the present context, this expression for  $k$  may also be viewed as an average value between those given by the two-center return conditions given in (30). For the specific parameters in this work, this yields  $p_{(1)||} + p_{(2)||} \simeq (1.45N - 0.849)\sqrt{U_p}$ . This estimate is in good agreement with the maxima and the minima displayed in Fig. 1.(b).

Interestingly, the distributions obtained from the transition probability  $|M_{jj} + M_{j\nu}|^2$ , with  $j = 1, 2$  and  $j \neq \nu$ , agree with the overall interference condition (17). This is shown in Figs. 1.(c) and 1.(e), and is due to the fact that one may rewrite the sum of such terms as  $\exp[\pm i\mathbf{k} \cdot \mathbf{R}/2] \cos[(\mathbf{p}_{(1)} + \mathbf{p}_{(2)} - \mathbf{k}) \cdot \mathbf{R}/2]$ . Apart from an overall phase factor, this is the same interference condition as if all transition amplitudes are taken. This latter case is shown in Fig. 1.(g), for comparison. Physically, the term  $M_{jj}$  corresponds to the orbits in which the first electron is freed at and subsequently rescatters off a specific center  $C_j$ , while  $M_{j\nu}$  gives the process in which it reaches the continuum at  $C_j$  and returns to the other center  $C_\nu$ . This suggests that these processes are the most relevant in determining the interference patterns from NSDI in a molecule.

On the other hand, if we consider scattering scenarios ending at the same center, the electron-momentum distributions resemble very much those obtained for the single-atom case, namely isotropic distributions centered near  $p_{(1)||} = p_{(2)||} = \pm 2\sqrt{U_p}$ . This holds regardless of whether one or two centers are involved, and can be seen in Figs. 1.(d) and 1.(f). In each panel, both one and two center processes are considered. However, interference fringes are absent. This is consistent with the double-slit physical picture, which relates the existence of the interference maxima

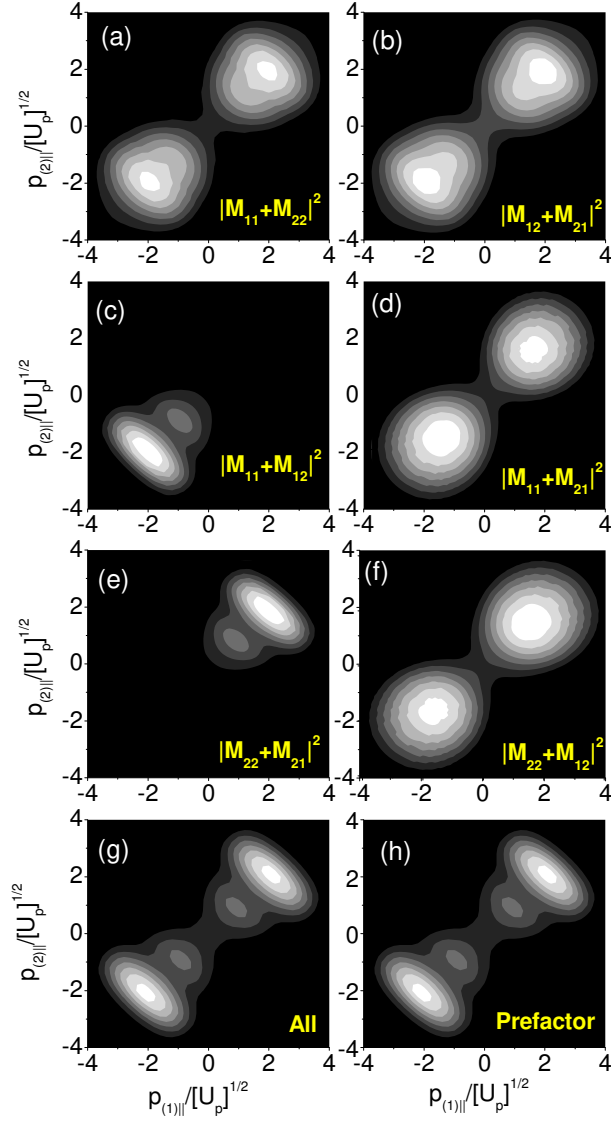


**Figure 2.** Contributions from different scattering scenarios to the electron momentum distributions as functions of the momentum components  $(p_{(1)\parallel}, p_{(2)\parallel})$  parallel to the laser-field polarization. The distributions have been computed in the length gauge and for a symmetric combination of 1s orbitals. The remaining parameters are the same as in the previous figure. The upper panels display the contributions from topologically similar scattering scenarios, involving only one or two centers, i.e., the transition probabilities  $|M_{11} + M_{22}|^2$  and  $|M_{12} + M_{21}|^2$  [panels (a) and (b), respectively]. In panels (c) and (d), we display the contributions from the processes starting and ending at center  $C_1$ , respectively (transition probabilities  $|M_{11} + M_{12}|^2$  and  $|M_{11} + M_{21}|^2$ , respectively). Panels (e) and (f) depict the contributions  $|M_{22} + M_{21}|^2$  and  $|M_{12} + M_{22}|^2$  from those starting and ending at  $C_2$ , respectively. The sum  $|M_{11} + M_{12} + M_{21} + M_{22}|^2$  of all contributions are provided in panel (g). For comparison, panel (h) has been computed using the prefactors (8) and (11) and the single-atom saddle-point equations.

and minima to photoelectron emission in spatially separated centers. This can also be seen by rewriting these contributions as  $\exp[\pm i(\mathbf{p}_{(1)} + \mathbf{p}_{(2)} - \mathbf{k} \cdot \mathbf{R}/2)]V_{\mathbf{k}0}$ . The form factor  $V_{\mathbf{k}0}$  does not lead to well-defined interference patterns, so that the distributions are very similar to those obtained in the single-atom case (for discussions see [19, 20]). Finally, we observe that Figs. 1.(d) and 1.(f) are practically identical. This means that the condition  $|M_{11} + M_{21}|^2 = |M_{22} + M_{12}|^2$  holds $\S$ . Intuitively, this is expected, as the transition amplitudes  $M_{j1}(j = 1, 2)$  are the complex conjugates of  $M_{j2}$ . The same holds for Figs. 1.(c) and 1.(e), which expresses the fact that  $|M_{11} + M_{12}|^2 = |M_{22} + M_{21}|^2$ .

The length-gauge counterparts of the distributions discussed above are presented in Fig. 2. In this case, we expect a different interference condition, according to Eq. (17). Furthermore, an inspection of the saddle-point equations shows that there exist additional potential-energy terms which lower or increase the barrier through which the first electron tunnels out. These energy shifts will influence the electron-momentum distributions, as we will discuss subsequently.

In the upper panels, we consider topologically similar scattering scenarios, involving only one or two centers [Figs. 2.(a) and 2.(b), respectively]. In contrast to the velocity-gauge situation, these distributions exhibit at most a slight distortion, as compared to the single-atom case. Sharp interference fringes, however, are absent. This is a consequence of the above-mentioned potential-energy shifts. Such shifts alter the potential-energy barriers in such a way that is much more probable for the first electron to tunnel out from a specific center of the molecule. Hence, the processes starting from a center  $C_j$  in the molecule will be far more prominent than those starting from the other center  $C_\nu(\nu \neq j)$  and there will be no sharp fringes. For the parameters employed in this figure, we estimate a difference of roughly one order of magnitude between each transition amplitude. A similar effect was present for high-order harmonic generation and has been discussed in detail in Ref. [9].

Also in the length gauge, the transition amplitudes  $M_{jj} + M_{j\nu}$  related the processes starting at the same center and ending at different centers lead to the same interference condition as the overall prefactors (8) and (11), apart from a phase factor  $\exp[\pm i\xi]$ , with  $\xi = [\mathbf{k} + \mathbf{A}(t')] \cdot \mathbf{R}/2$ . There are, however, some major quantitative differences, due to the fact that  $\text{Im}[t'] \neq 0$ . This leads to a non-vanishing imaginary part in  $\xi$ , which, depending on the field, will enhance the yield for a center  $C_j$  and suppress it for the other center  $C_\nu$  in the molecule. As the field reverses its sign, the contributions from  $C_j$  will be suppressed and those from the other center enhanced. This leads to strongly asymmetric electron momentum distributions, and may be interpreted as another consequence of the additional potential-energy shifts, which are present only in the length-gauge formulation of the SFA.

The above-stated features are explicitly shown in Figs. 2.(c) and 2.(e), starting from  $C_1$  and  $C_2$ , respectively. In the former case [Figs. 2.(c)], the yield is strongly suppressed in the region of positive parallel momentum. This is due to the fact that the additional potential energy shifts suppresses tunneling ionization for all the orbits starting from  $C_1$ . As the field reverses its sign, i.e., when  $t' \rightarrow t' + T/2$ , the barrier will be sunk by these shifts. This explains the much larger yield in the negative momentum region. Fig. 2.(e), which is the mirror image of Figs. 2.(c) with respect

$\S$  We have verified, by a series of numerical computations, that this condition only holds in practice. This is a consequence of the fact that the start time  $t'$  exhibits a non-vanishing imaginary time, and that, according to the saddle-point Eqs. (29), (30), the intermediate momentum depends on this variable. The relative differences in the yields, however, is less than 0.2%.

to  $(p_{1||}, p_{2||}) \rightarrow (-p_{1||}, -p_{2||})$ , exhibits the consequences of the opposite effect: for the time  $t'$ , the barrier is sunk for  $C_2$ . This leads to enhanced distributions in the positive momentum regions. After half a cycle, as the field changes its signs, the barrier will be lifted and the contributions in the negative momentum region suppressed. A similar effect has been observed for high-order harmonic generation [9, 10], In particular, in [10], apart from modified saddle-point equations, we have employed effective prefactors and single-atom saddle-point equations in order to mimic the interference between different processes. Also in the latter case, we observed different orders of magnitude for processes starting at different centers.

Therefore, in contrast to the velocity-gauge situation, the processes starting at a particular center of the molecule do not lead to the same distributions as if all four terms in Eq. (20) are taken. These latter results are displayed in Fig. 2.(g). For comparison, in Fig. 2.(h), we also provide the outcome of the computations using single-atom saddle-point equations and the prefactor (11) and (8). Finally, if the processes starting at different centers, but ending at the same center lead to distributions qualitatively similar than those observed in the single-atom case [see Fig. 2.(d) and (f)]. Similarly to the velocity-gauge situation, the terms can be combined in  $\exp[\pm i(\mathbf{p}_{(1)} + \mathbf{p}_{(2)} - (\mathbf{k} - \mathbf{A}(t)) \cdot \mathbf{R}/2)] \cos[\mathbf{k} + \mathbf{A}(t')]$ . Even if the extra dependence on the vector potential influences the distributions, qualitatively, similar conclusions hold. However, there is a slight asymmetry with respect to the reflection  $(p_{1||}, p_{2||}) \rightarrow (-p_{1||}, -p_{2||})$  due to the fact that the times  $t, t'$  are complex. Once more, the contributions of the processes ending at a particular center  $C_j$  are the mirror image those ending at the other center  $C_\nu$ .

In the following, we explicitly show that the above-mentioned asymmetries are caused by  $\text{Im}[t]$ , and  $\text{Im}[t']$ . For that purpose, in Fig. 3, we plot the counterparts of Fig. 2(c)-2(f) employing only the real parts of such times. In this case, the contributions of the orbits starting at the same center are symmetric, i.e., the condition  $|M_{11} + M_{12}|^2 = |M_{22} + M_{21}|^2$  holds [see Figs. 3.(a) and 3.(c)]. The contributions ending at the same center, depicted in Figs. 3.(b) and 3.(d), also exhibit the symmetry  $|M_{11} + M_{21}|^2 = |M_{22} + M_{12}|^2$ . In these computations, instead of employing modified saddle-point equations, we grouped the separate transition amplitudes in the effective prefactors

$$V_{C_j}^{\text{start}}(\{\mathbf{p}_{(n)}\}, \mathbf{k}) \sim \exp[i(-1)^j [\mathbf{k} + \mathbf{A}(t')] \cdot \mathbf{R}/2] \quad (34)$$

$$\times \cos[(\mathbf{p}_{(1)} + \mathbf{p}_{(2)} - \mathbf{k} + \mathbf{A}(t)) \cdot \mathbf{R}/2]$$

and

$$V_{C_j}^{\text{end}}(\{\mathbf{p}_{(n)}\}, \mathbf{k}) \sim \exp[i(-1)^j (\mathbf{p}_{(1)} + \mathbf{p}_{(2)} - \mathbf{k} + \mathbf{A}(t)) \cdot \mathbf{R}/2] \quad (35)$$

$$\times \cos[\mathbf{k} + \mathbf{A}(t')]$$

mimicking the processes starting and ending at a center  $C_j$ , respectively, and employed single-atom saddle-point equations (see Ref. [10] for details on this procedure). The imaginary parts of  $t, t'$  were removed in the prefactors only.

#### 4. Conclusions

We have made a detailed analysis of the different scattering scenarios in laser-induced nonsequential double ionization of diatomic molecules, within the framework of the strong-field approximation. We assumed that the second electron is dislodged by electron-impact ionization and employed saddle-point methods. The semiclassical

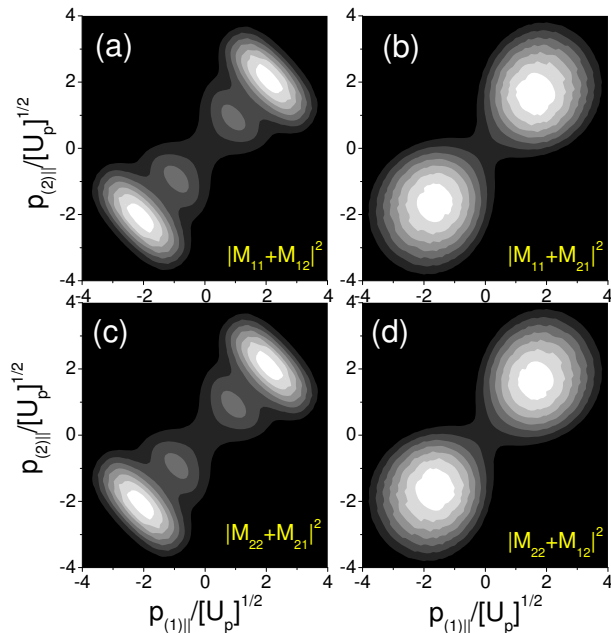


**Figure 3.** Transition probabilities starting and ending at the same centers, considering only the real parts of  $t, t'$ , as functions of the momentum components  $(p_{(1)\parallel}, p_{(2)\parallel})$  parallel to the laser-field polarization, for the same parameters as in Fig. 2. Panels (a), and (b) exhibit the contributions from the processes starting and ending at center  $C_1$  (transition probabilities  $|M_{11} + M_{12}|^2$  and  $|M_{11} + M_{21}|^2$ , respectively), while panels (c) and (d) depict the contributions  $|M_{21} + M_{22}|^2$  and  $|M_{12} + M_{22}|^2$  from those starting and ending at  $C_2$ , respectively.

action has been modified in order to account for four different physical processes. In two of them, the first electron is released and rescatters off the same center  $C_j$  ( $j = 1, 2$ ). In the remaining processes, it leaves from a center  $C_j$  and rescatters with a different center  $C_\nu$ ,  $\nu \neq j$ .

We placed particular emphasis on the quantum interference between such processes, and on how it affects the differential electron momentum distributions, as functions of the momentum components  $p_{(n)\parallel}$  ( $n = 1, 2$ ) parallel to the laser-field polarization. For that purpose, we considered parallel-aligned molecules, for which the interference patterns are sharpest [19]. We found that the contributions of the processes in which the first electron starts at the same center  $C_j$ , regardless of whether it returns to the site of its release or to the other center  $C_\nu$ , yield interference patterns which fulfill the overall interference condition (17). There exist, however, differences for both velocity and length-gauge formulations of the SFA. Indeed, while in the velocity gauge the contributions of the above-stated orbits leads to the same distributions as in the overall case, this affirmative cannot be made in the length-gauge situation. In this latter case, there are additional potential energy shifts, which sink or increase the potential barrier through which the first electron tunnels. This favors the contributions of a particular center in the molecule, and suppresses those from

the other center. As the electric field changes sign, so do the shifts. This leads to asymmetries in the electron-momentum distributions.

The quantum interference between other types of processes leads either to quite different interference patterns, or to momentum distributions that strongly resemble those obtained for a single atom. In particular, a resemblance to single-atom distributions is observed if only the processes for which the first electron rescatters at the same center  $C_j$  are considered. The fact that interference fringes are absent is in agreement with the double-slit physical picture, as there is no electron emission at spatially separated centers for such processes.

Sharp interference fringes, on the other hand, are observed if we consider topologically similar scattering scenarios, involving either one or two centers, and the velocity gauge. This is expected since, in this case, the first electron rescatters at spatially separated centers. It is worth noticing, however, that the interference patterns, and thus the electron-momentum distributions, look quite different from those obtained if all contributions are taken. Physically, this indicates that we can not single out the interference between such processes as being the most relevant. In the length gauge, in principle, there are also interference patterns. In practice, however, we only see slight distortions, as compared to the single-atom case. This is due to the additional potential-energy shifts, which sink or increase the potential barrier through which the first electron must tunnel in order to reach the continuum. Hence, the contributions starting at a center  $C_j$  in which the barrier has been sunk will be far more prominent than those from a center  $C_\nu$  in which it has been raised.

The above-stated issues contribute to the present controversy involving the above-mentioned potential-energy shifts [7, 9, 11, 18, 26, 27, 28]. Indeed, it is not clear whether they are only an artifact of the strong-field approximation, or whether they possess some physical meaning. For instance, in [9, 27] it has been shown that, if such shifts are not present, there exists a breakdown in the double-slit interference patterns for high-order harmonic generation. Specifically in [27], it was argued that, for small internuclear distances, there is no physical justification for dressing the electronic bound states with a linear phase factor. In fact, according to [27] a quadratic phase factor would be the correct form of dressing, and would physically correspond to the quadratic Stark effect. On the other hand, in [7], it was shown that, for internuclear distances of the order of the electron excursion amplitude, the additional potential-energy shifts led to an unphysical increase in the high-harmonic intensities and cutoff energies. Furthermore, in [28] it was demonstrated that a linear dressing in the electronic bound states is necessary in order cancel out the extra potential-energy shifts and to restore, among others, translation invariance. In this specific work, one argument against the existence of the potential-energy shifts would be that, for a homonuclear molecule, one would intuitively expect the symmetries  $|M_{11} + M_{21}|^2 = |M_{22} + M_{12}|^2$  and  $|M_{11} + M_{12}|^2 = |M_{22} + M_{21}|^2$  to hold. Due to the fact that, in the length gauge, the imaginary part of  $t'$  is shifted in different ways for different centers in molecule, we have seen that, instead, the distributions starting at a specific center  $C_j$  are a reflection upon  $(p_{1||}, p_{2||}) \rightarrow (-p_{1||}, -p_{2||})$  of those starting at the other center  $C_\nu$ .

Finally, we would like to comment on the similarities and differences between the present results and those reported in our previous work [9, 10], on the double-slit quantum interference for HHG in diatomic molecules. Therein, even though there was strong evidence that the interference maxima and minima in the spectra were due to the transition probability  $|M_{jj} + M_{j\nu}|^2$ , related to the interference of the

orbits starting at the same center and finishing at different centers, there were several ambiguities. Firstly, this information could only be extracted in the length gauge, due to limitations of the SFA. Within this approach, there is a breakdown in the interference patterns if the velocity gauge is employed to compute the high-harmonic yield. Furthermore, similarly to the present case, the length-gauge formulation of the SFA exhibits additional potential-energy shifts which make the ionization probability far more probable from one center than from the other. This holds even for very small internuclear distances [10], and could be the reason why the interference patterns would not be present also in the transition probabilities  $|M_{jj} + M_{\nu\nu}|^2$ , or  $|M_{j\nu} + M_{\nu j}|^2$ , involving one or two-center orbits, respectively. By providing an additional pathway for the electron to reach the continuum, using attosecond pulses, we could verify that these processes led to maxima and minima if the potential-energy shifts could be overcome. Since, however, we were modifying the physics of the problem, we could not reach a definitive conclusion.

Fortunately, many of these ambiguities are not present for laser-induced nonsequential double ionization. This is possibly due to the fact that this phenomenon intrinsically involves electron-electron correlation, whereas high-order harmonic generation may be modeled within the single-active electron approximation. Indeed, although the distributions computed in this work employing the topologically similar scattering scenarios may, in some cases, exhibit interference patterns, these do not agree with the overall interference conditions. Furthermore, in contrast to the high-order harmonic case, there is no breakdown of the interference patterns in the velocity-gauge situation. This allows one to assess the influence of the topologically similar scenarios on the NSDI electron momentum distributions in the absence of the above-mentioned potential energy shifts. Finally, it is rather interesting that, in the length gauge, the influence of the potential energy shifts can be directly mapped into the electron momentum distributions for the processes starting at the same center. For instance, if the electron started at a center  $C_1$ , for the parameters used in this work, there is a suppression of the yield in the positive momentum region and an enhancement for positive parallel momentum, whereas if it has started at  $C_2$  the situation will be reversed, i.e., there will be an enhancement in the region of positive parallel momenta and a suppression for  $p_{(n)\parallel} < 0$  ( $n = 1, 2$ ). This means that different potential energy shifts lead to an enhancement or a suppression of the distributions in distinct momentum regions.

Hence, if these processes could be isolated in a realistic scenario, one could in principle determine from which side of the molecule the first electron reached the continuum. Furthermore, if no asymmetry is observed, the existence of the potential-energy shifts and the validity of the length-gauge SFA electron momentum distributions could be ruled out in the context of diatomic molecules. For that purpose, it would be necessary to suppress all the the orbits starting from one center of the molecule in the overall distributions . This could be achieved if, for instance, the system is prepared in such a way that the initial state of the first electron is localized in one center of the molecule, or if the external laser field is taken as a few-cycle pulse with an adequate choice of carrier-envelope phase.

## Acknowledgments

We are grateful to T. Shaaran, C. Ruiz, X. Liu and W. Yang for useful discussions. This work has been financed by the UK EPSRC (Advanced Fellowship, Grant no.



EP/D07309X/1).

## References

- [1] Niikura H, Légaré F, Hasbani R, Bandrauk A D, Ivanov M Yu, Villeneuve D M and Corkum P B 2002 *Nature* **417** 917  
 Niikura H, Légaré F, Hasbani R, Ivanov M Yu, Villeneuve D M and Corkum P B, 2003 *Nature* **421** 826  
 Itatani J, Levesque J, Zeidler D, Niikura H, Pépin H, Kieffer J C, Corkum P B and Villeneuve D M, 2004 *Nature* **432** 867  
 Baker S, Robinson J S, Haworth C A, Teng H, Smith R A, Chirilă C C, Lein M, Tisch J W G, Marangos J P, 2006 *Science* **312** 424
- [2] Corkum P B, 1993 *Phys. Rev. Lett.* **71** 1994  
 Kulander K C, Schafer K J, and Krause J L in: B. Piraux et al. eds., *Proceedings of the SILAP conference*, (Plenum, New York, 1993)
- [3] Scrinzi A, Ivanov M Yu, Kienberger R, and Villeneuve D M, 2006 *J. Phys. B* **39** R1
- [4] Lein M, Hay N, Velotta R, Marangos J P, and Knight P L, 2002 *Phys. Rev. Lett.* **88** 183903  
 Lein M, Hay N, Velotta R, Marangos J P, and Knight P L 2002 *Phys. Rev. A* **66** 023805  
 Spanner M, Smirnova O, Corkum P B and Ivanov M Yu, 2004 *J. Phys. B* **37** L243
- [5] Kopold R, Becker W and Kleber M, 1998 *Phys. Rev. A* **58** 4022
- [6] Usachenko V I, Pyak P E, and Chu Shih-I, 2006 *Laser Phys.* **16** 1326
- [7] Chirilă C C and Lein M, 2006 *Phys. Rev. A* **73** 023410
- [8] Hetzheim H, Figueira de Morisson Faria C, and Becker W 2007 *Phys. Rev. A* **76** 023418
- [9] Figueira de Morisson Faria C, 2007 *Phys. Rev. A* **76** 043407
- [10] Figueira de Morisson Faria C, 2007, arXiv: 0810.5251
- [11] Busuladžić M, Gazibegović-Busuladžić A, Milošević D B, and Becker W 2008 *Phys. Rev. Lett.* **100** 203003
- [12] Lewenstein M, Balcou Ph, Ivanov M Yu, L'Huillier A and Corkum P B, 1994 *Phys. Rev. A* **49** 2117  
 Becker W, Long S, and McIver J K 1990 *Phys. Rev. A* **41** 4112  
 Becker W, Long S, and McIver J K 1994 *Phys. Rev. A* **50** 1540  
 Lewenstein M, Kulander K C, Schafer K J and Bucksbaum P 1995 *Phys. Rev. A* **51** 1495
- [13] Usachenko V I, and Chu S I 2005 *Phys. Rev. A* **71** 063410
- [14] Lein M 2005 *Phys. Rev. Lett.* **94** 053004  
 Chirilă C C and Lein M 2006 *J. Phys. B* **39** S437  
 Chirilă C C and Lein M, 2007 *J. Mod. Opt.* **54** 1039
- [15] Muth-Böhm J, Becker A, and Faisal F H M, 2000 *Phys. Rev. Lett.* **85** 2280  
 Jarón-Becker A, Becker A, and Faisal F H M 2004 *Phys. Rev. A* **69** 023410  
 Requate A, Becker A and Faisal F H M 2006 *Phys. Rev. A* **73** 033406
- [16] Kjeldsen T K and Madsen L B 2004 *J. Phys. B* **37** 2033  
 Kjeldsen T K and Madsen L B 2005 *Phys. Rev. A* **71** 023411  
 Kjeldsen T K and Madsen L B 2005 *Phys. Rev. Lett.* **95** 073004  
 Kjeldsen T K, Bisgaard C Z, Madsen L B, Stapelfeld H 2005 *Phys. Rev. A* **71** 013418  
 Madsen C B and Madsen L B 2006 *Phys. Rev. A* **74** 023403
- [17] Zhou X, Tong X M, Zhao Z X and Lin C D 2005 *Phys. Rev. A* **71** 061801(R)  
 Zhou X, Tong X M, Zhao Z X and Lin C D 2005 *Phys. Rev. A* **72** 033412
- [18] Milošević D B, 2006 *Phys. Rev. A* **74** 063404
- [19] Figueira de Morisson Faria C, Shaaran T, Liu X and Yang W, arXiv:0806.4856 [atom.ph]
- [20] Eremina E, Liu X, Rottke H, Sandner W, Schätzel M G, Dreischuch A, Paulus G G, Walther H, Moshhammer R and Ullrich J 2004 *Phys. Rev. Lett.* **92** 173001
- [21] Zeidler D, Staudte A, Bardon A B, Villeneuve D M, Dörner R, and Corkum P B 2005 *Phys. Rev. Lett.* **95** 203003
- [22] Fring A, Kostyrykin V and Schrader R 1996 *J. Phys. B.* **29** 5651  
 Bauer D, Milošević D B and Becker W 2005 *Phys. Rev. A* **72** 023415
- [23] Figueira de Morisson Faria C, Schomerus H and Becker W 2002 *Phys. Rev. A* **66** 043413
- [24] Figueira de Morisson Faria C, Schomerus H, Liu X, and Becker W 2004 *Phys. Rev. A* **69** 043405
- [25] Figueira de Morisson Faria C, and Lewenstein M 2005 *J. Phys. B* **38** 3251
- [26] Smirnova O, Spanner M and Ivanov M 2006 *J. Phys. B* **39** S307
- [27] Smirnova O, Spanner M and Ivanov M 2007 *J. Mod. Opt.* **54** 1019
- [28] Becker W, Chen J, Chen S G, and Milošević D B, 2007 *Phys. Rev. A* **76**, 033403
- [29] Chipperfield L, 2008, Ph.D. thesis, Imperial College London